Structural Features and Light-Dependent Changes in the Sequence 306−322 Extending from Helix VII to the Palmitoylation Sites in Rhodopsin: A Site-Directed Spin-Labeling Study[†,‡]

Christian Altenbach,[§] Kewen Cai,[||] H. Gobind Khorana,*[,||] and Wayne L. Hubbell*[,§]

Jules Stein Eye Institute and Department of Chemistry and Biochemistry, University of California, Los Angeles, California 90095-7008, and Departments of Biology and Chemistry, Massachusetts Institute of Technology, 77 Massachusetts Avenue, Cambridge, Massachusetts 02139

Received January 4, 1999; Revised Manuscript Received April 8, 1999

ABSTRACT: Sixteen single-cysteine substitution mutants of rhodopsin were prepared in the sequence 306−321 which begins in transmembrane helix VII and ends at the palmitoylation sites at 322C and 323C. The substituted cysteine residues were modified with a selective reagent to generate a nitroxide side chain, and the electron paramagnetic resonance spectrum of each spin-labeled mutant was analyzed in terms of residue accessibility and mobility. The periodic behavior of these parameters along the sequence indicated that residues 306−314 were in a regular α-helical conformation representing the end of helix VII. This helix apparently extends about 1.5 turns above the surface of the membrane, with one face in strong tertiary interaction with the core of the protein. For the segment 315−321, substituted cysteine residues at 317, 318, 320, and 321 had low reactivity with the spin-label reagent. This segment has the most extensive tertiary interactions yet observed in the rhodopsin extra-membrane sequences at the cytoplasmic surface. Previous studies showed the spontaneous formation of a disulfide bond between cysteine residues at 65 and 316. This result indicates that at least some of the tertiary contacts made in the 315−321 segment are with the sequence connecting transmembrane helices I and II. Photoactivation of rhodopsin produces changes in structure detected by spin labels at 306, 313, and 316. The changes at 313 can be accounted for by movements in the adjacent helix VI.

Rhodopsin is the dim light photoreceptor of the vertebrate retina and was the first characterized member of the large family of GPCR's[1] (*2*−*4*). All GPCR's are believed to have seven transmembrane helical segments. A secondary structural model of rhodopsin showing an assignment for the transmembrane helical segments is given in Figure 1. The extramembranous sequences linking helices III to IV, V to VI, and VII to the palmitoylation sites at 322 and 323 are involved in the binding and/or activation of the visual G protein, G_T (*12*−*16*). In the dark state, certain residues of these sequences are apparently sequestered within the tertiary fold of rhodopsin, becoming available to G_T only after photoisomerization of the 11-*cis*-retinal chromophore triggers a conformational change in rhodopsin (*2*−*4*).

The structure of rhodopsin and the details of the light-activated conformational change have been the focus of numerous biochemical and biophysical investigations. Recently, a model for the helix packing of rhodopsin has been constructed on the basis of low-resolution electron density

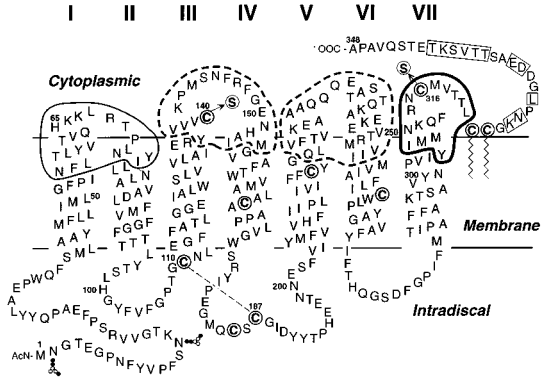

FIGURE 1: A secondary structure model of rhodopsin showing the residues in the cytoplasmic region where single-cysteine substitutions and nitroxide spin labels have been introduced. The sequence investigated by nitroxide spin labeling in the present study is outlined with a bold line. The sequences included within dashed lines are those previously investigated (*5*−*8*). The sequence highlighted by a thin line, and the residues boxed in the C-terminal domain, are the subject of accompanying papers (*1*, *9*−*11*). In total, these studies include 100 single-cysteine substitutions and their spin-labeled derivatives that cover the entire cytoplasmic face of the molecule. In all single-cysteine substitution mutants, the reactive native cysteines at residues 140 and 316 were replaced by serine, as indicated. The secondary structures in the extramembranous segments and the location of the cytoplasmic membrane−aqueous interface relative to the helices are based on the above referenced studies.

[†] Research reported here was supported by NIH Grants EY05216 (W.L.H.) and GM28289 (H.G.K.), the Jules Stein Professorship Endowment (W.L.H.), and a grant from the Bruce Ford Bundy and Anne Smith Bundy Foundation (W.L.H.).

[‡] This is paper 31 in the series "Structure and Function in Rhodopsin". The preceding paper is ref *1*.

* To whom correspondence should be addressed.

[§] University of California.

[||] Massachusetts Institute of Technology.

[1] Abbreviations: DM, dodecyl maltoside; EPR, electron paramagnetic resonance; GPCR, G-protein-coupled receptor; G_T, transducin; NiEDDA, Ni(II) ethylenediaminediacetate; 4-PDS, 4,4′-dithiopyridine; SDSL, site-directed spin labeling.

10.1021/bi9900121 CCC: $18.00
Published on Web 05/26/1999

maps derived from cryoelectron microscopy (*17*−*18*). Structural models for the extramembranous segments at the cytoplasmic surface have been proposed on the basis of NMR studies of synthetic peptides of the same sequence (*19*−*22*). A model for the tertiary structure of the cytoplasmic domain based on NMR data of the peptide segments has also been proposed (*23*). Mutagenesis experiments using metal ion binding to double-histidine replacements provided some information on the proximity of rhodopsin helices in the dark state (*24*).

Cysteine scanning mutagenesis and double-cysteine substitution mutagenesis form the basis for a powerful experimental approach that has been recently applied to analyze the structure and function in rhodopsin (*6*−*8*, *25*−*29*). The general strategy relies on an analysis of the following: (1) functional perturbation due to the cysteine substitution; (2) reactivity of the substituted cysteine; (3) cross-linking of cysteines in double mutants; and (4) SDSL data. Functional perturbation due to cysteine substitution can be used to identify residues essential for structure and/or function, while the chemical reactivity of single-cysteine mutants provides general information on site accessibility (*30*). Functional perturbation and cysteine reactivity have been previously employed to explore the extramembranous sequences connecting helices III to IV (*5*) and helices V to VI in rhodopsin (*7*), and the C-terminal domain (*28*). Extensions of these studies to the sequence connecting helices I and II and the sequence connecting helix VII to the palmitoylation sites are the subjects of accompanying papers (*1*, *9*). The spontaneous cross-linking rates between cysteine residues in double mutants of rhodopsin have provided information on residue proximity (*26*, *27*).

Finally, for SDSL applications, single- and double-cysteine mutants are used to attach a paramagnetic nitroxide side chain to the protein. The EPR of such labeled proteins provide direct information on residue solvent accessibility, sequence-correlated secondary structure, protein topography, and interresidue distances with a real-time resolution sufficient to observe protein motions during function (see refs *31*−*33* for recent reviews). In previous publications, SDSL methods were used to explore the structure and light-dependent changes in rhodopsin sequences that connect transmembrane helices III to IV (*6*, *25*, *34*) and V to VI (*8*, *26*). In accompanying papers, the structure of the sequence connecting transmembrane helix I to II (*10*) and the C-terminal domain (*11*) are analyzed by SDSL.

The present paper extends the SDSL analysis of rhodopsin to include the sequence 306−321. This sequence encompasses portions of transmembrane helix VII and the extramembranous segment that extends to the palmitoylation sites at residues 322 and 323 (Figure 1). This is a particularly interesting region in rhodopsin, because Lys296 on helix VII is the site of the protonated Schiff base that links the 11-*cis*-retinal chromophore to the protein. The protonated Schiff base is involved in salt bridge formation with E113 on helix III (*35*−*37*), an interaction that is believed to be an essential component of the light-activated rhodopsin conformational switch (*38*−*39*). The extramembranous segment of the 306−321 sequence has been referred to as a "fourth cytoplasmic loop" and is involved in G_T activation (*13*). The results presented here support the existence of a regular helical segment extending from residue 306 to approximately 314,

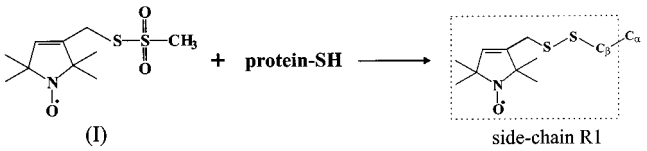

FIGURE 2: Reaction of the methanethiosulfonate spin label (I) to produce the nitroxide side chain designated R1.

corresponding to the cytoplasmic end of helix VII. The helix crosses from a nonpolar to an aqueous environment in the neighborhood of residues 308−309, indicating that helix VII extends into the aqueous phase. The sequence 315−321 is apparently in strong tertiary interaction with the remainder of rhodopsin. Significant structural changes are observed after light activation at residues 306 and 313 on the buried surface of helix VII and at 316, as reported earlier (*25*−*27*).

EXPERIMENTAL SECTION

Preparation and Spin Labeling of Rhodopsin Mutants. The single-cysteine substitution mutants in the region 306−321 used in this study were prepared and purified in DM solution as described in a accompanying paper (*1*) and were spin-labeled with (1-oxy-2,2,5,5 tetramethylpyrrolin-3-methyl) methanethiosulfonate (I) (a gift from Prof. Kálmán Hideg, University of Pécs, Hungary) as described elsewhere (*28*). The nitroxide side chain generated by this reaction is referred to as R1 (Figure 2). Spin-labeled mutants will be designated by giving the original residue and the sequence number followed by R1, or just the sequence number followed by R1. Thus, F313R1 or 313R1 is a mutant with the native phenylalanine at 313 replaced by the nitroxide side chain R1. The spin-labeled mutants were concentrated in the DM solution and loaded into TPX or quartz capillaries, and X-band EPR spectra and power saturation data were collected as previously described (*40*).

RESULTS

Structure and Light-Induced Changes in the Sequence 306−*321.* Figure 3 shows the EPR spectra recorded at room temperature both in the dark (solid trace) and after photoexcitation (dashed trace) for the various spin-labeled mutants in the region 306−321. The spectra of Y306R1, I307R1, and M317R1 are relatively noisy, apparently due to a low reactivity of the cysteine residues at these positions with the spin-label reagent (I). Only very weak signals were obtained after reaction of mutants V318C, T320C, and L321C with (I). The spectra are too noisy to be of use and are not shown. These results are consistent with the extremely low reactivity of the Y306C, I307C, M317C, V318C, T320C, and L321C mutants with 4-PDS (*1*), and they suggest that these sites are buried within the structure.

The term "mobility" is a qualitative descriptor of the dynamic modes of R1 in the protein as reflected by general features of the EPR spectra shown in Figure 3 (*41*). For example, the large separation between the well-resolved outer hyperfine extrema in the EPR spectra of 306R1, 310R1, and 313R1 indicate that the nitroxides are strongly immobilized by interaction with the protein. These sites are likely to be buried in the protein interior. The spectra of 307R1, 314R1, 315R1, and 316R1 also reflect the presence of a population of spin that is relatively immobilized, judging by the intensity

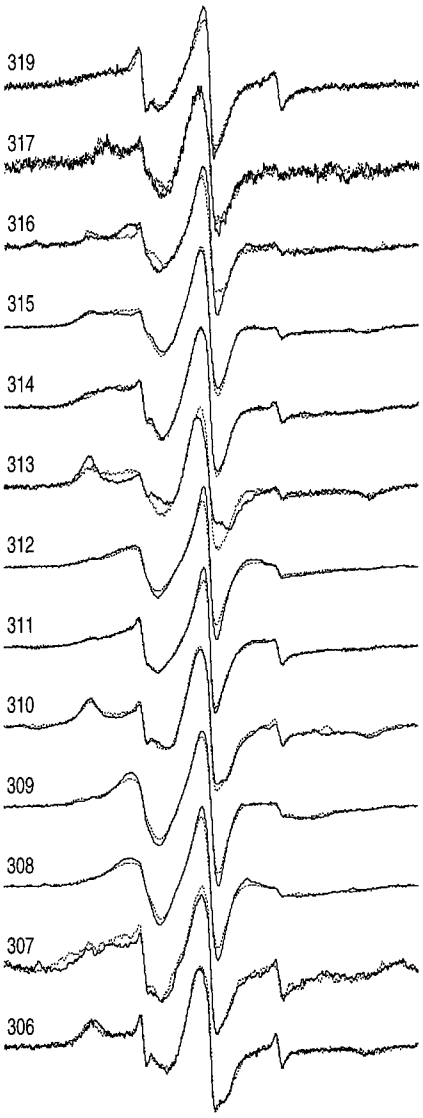

FIGURE 3: EPR spectra in the dark (solid trace) and after photoactivation (dotted trace) for each of the spin-labeled mutants.

in the low- and high-field regions of the spectra. On the other hand, the spectra of 308R1, 309R1, 311R1, and 312R1 are dominated by components characteristic of R1 side chains with relatively high mobility. The inverse line width of the central $m_I = 0$ resonance line (ΔH^{-1}) and the inverse spectral second moment ($<H^2>^{-1}$) may be used as crude descriptors of nitroxide mobility, although they do not distinguish individual components in complex spectra (*41*). In the usual case of multicomponent spectra, the ΔH^{-1} measure more heavily weighs the most mobile component, while $<H^2>^{-1}$ more heavily weighs the least mobile component. We use ΔH^{-1} in the present study because the poor baseline in some of the spectra would cause large errors in the second moment. Figure 4A shows a plot of ΔH^{-1} for the spin-labeled mutants in the range 306−316 (solid symbols) together with a periodic function of period 3.6 for reference. It is apparent that the residue mobility is periodic in position to at least residue 314, and the period is close to that of an α-helix.

After photoexcitation to produce the MII state, there are subtle changes in the EPR spectra of most of the mutants, but the changes in Y306R1, F313R1, and C316R1 are the most significant. The change in C316R1 has been previously

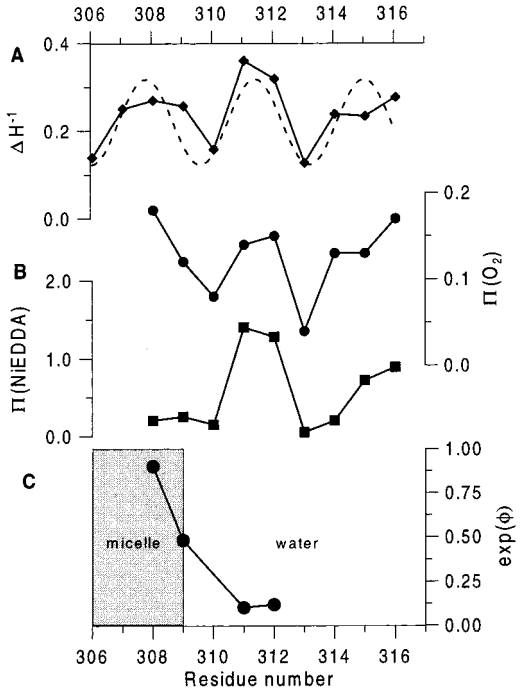

FIGURE 4: Mobility and accessibility of the R1 side chain in the sequence 306−316. (A) The mobility of the R1 side chain measured by the inverse of the central resonance line width, ΔH^{-1}. The dotted line has a period of 3.6 residues. (B) The accessibility to collision with molecular oxygen (●) and with NiEDDA (■). The concentration of NiEDDA was 20 mM, and for O_2 was that in equilibrium with air. (C) The function e^{Φ} for the exposed and mobile residues.

reported, and the result is reproduced here (*25*). For 306R1, there is an increase in the splitting of the outer hyperfine extrema, which could be due to either a decrease in mobility or an increase in polarity of the environment (*42*). For F313R1, photoexcitation produces a relative increase in intensity in regions of the spectrum corresponding to a more mobile state, while the opposite is the case at C316R1.

The solvent accessibility of side chains also provides valuable information on local protein structure. The solvent accessibility of R1 in a protein may be inferred from the collision frequency of the nitroxide with paramagnetic reagents in solution. For membrane proteins, two different paramagnetic reagents are employed, one polar and the other nonpolar. For the nonpolar reagent, O_2 is selected because of its higher solubility in the hydrophobic interior of membranes and micelles than in water. NiEDDA is selected as the polar reagent for these studies, because it has a high solubility in water and a very low solubility in hydrophobic media. An accessibility parameter, Π, proportional to the collision frequency of the nitroxide with either reagent, can be estimated by power saturation techniques (*43*). Figure 4B shows values for $\Pi(O_2)$ and Π(NiEDDA) for R1 as a function of sequence number in the range 308−316. Values for 306R1 and 307R1 were not determined due to the poor signal-to-noise. The values of $\Pi(O_2)$ rather closely parallel those of ΔH^{-1}; that is, the residues with the highest mobility are also the most exposed to collision with O_2. Residues 310R1 and 313R1 have the lowest accessibility to O_2, consistent with the assignment of those residues to buried sites based on mobility. Residues 308R1, 309R1, 311R1, 312R1, 314R1, 315R1, and 316R1 all have moderate to high accessibility, indicating their location on exposed surfaces

or loosely packed interior domains accessibly to O_2. The high values of Π(NiEDDA) unequivocally identify 311R1 and 312R1 as water-exposed sites. The low values of Π(NiEDDA), high values of $\Pi(O_2)$, and high mobility of 308R1 and 309R1 demonstrate the exposure of these sites at a surface of the protein solvated by the fluid hydrocarbon chains of the micelle interior. The low values of Π(NiEDDA) at 310R1 and 313R1 strengthen the conclusion reached above that these are both buried residues. The low Π(NiEDDA), relatively high $\Pi(O_2)$, and intermediate mobility suggest that 314R1 may lie at a loosely packed buried or tertiary contact site.

Topography in the Sequence 306−321. For a nitroxide on the surface of a protein in water, or in any other homogeneous solvent, the parameter $\Phi = \ln[\Pi(O_2)/\Pi(\text{NiEDDA})]$ is approximately constant, independent of the site at which the nitroxide is attached. This is because structural factors that influence $\Pi(O_2)$ have a similar effect on Π(NiEDDA), and site-specific effects cancel in forming the ratio that defines Φ (*44*).[2] For a nitroxide on the surface of a transmembrane protein, Φ is a linear function of depth from the membrane−water interface, apparently because concentration gradients of the reagents exist in the nonhomogeneous interior of the membrane (*44*). Thus, the slope of Φ undergoes an abrupt change across the boundary between the hydrophobic interior of the membrane and the aqueous phase, making it a useful parameter to locate positions in a protein sequence that lie in this boundary region (*6*, *8*).

For use in DM micelles, Φ is calibrated using spin-labeled phospholipids containing a nitroxide in the headgroup and at various points along a hydrocarbon chain solubilized in the micelle (*6*). For 20 mM NiEDDA and O_2 in equilibrium with air, a nitroxide in the polar headgroup region had $\Phi \approx 0$, defining the outer boundary of the interface, while a nitroxide in the micelle interior had $\Phi > 4$. For the same concentrations of NiEDDA and O_2, a fully water-exposed R1 residue on a water-soluble protein has $\Phi \approx -2.5$ (Altenbach and Hubbell, unpublished results). Because the range of Φ is relatively small through the diffuse micelle interface, it is convenient to employ e^{Φ} rather than Φ itself for graphical presentation. Figure 4C shows e^{Φ} as a function of position for R1 residues in the sequence 306−312 of rhodopsin. Only residues exposed to solvent with high mobility are included in the analysis.[2] According to these data and the calibrations mentioned above, residues 308 ($e^{\Phi} = 1$, $\Phi = 0$) and 309 ($e^{\Phi} = 0.5$, $\Phi = -.69$) lie in the diffuse headgroup region of the DM micelle. Residues 311 and 312 are apparently completely solvent-exposed ($e^{\Phi} = 0.125$, $\Phi = -2.1$). The e^{Φ} values for these latter residues are in close agreement with the average value of equivalent residues in the extramembranous sequence connecting helices V and VI in rhodopsin (*8*).

DISCUSSION

The periodic dependence of R1 side chain mobility and accessibility on sequence position suggests the existence of an α-helical segment extending from about residues 306 to 314 (Figures 3 and 4). Figure 5A shows the mobility, represented by the symbol **M**, $\Pi(O_2)$, represented by Π, and other data (see below) plotted on a helical wheel representation of the sequence. Accessibility to O_2 rather than NiEDDA is selected for structural analysis because NiEDDA has extremely low solubility in the micelle interior. Thus every residue in the micelle interior, whether exposed or buried, will have a very low Π(NiEDDA) and structural information is obscured. On the other hand, O_2 has finite solubility in both water and the micelle interior, and structural modulation of $\Pi(O_2)$ is readily apparent for all residues. In Figure 5A, the magnitudes of mobility and accessibility are color coded from red to yellow, red being the most immobilized and inaccessible. White circles indicate that the measurement was not made.

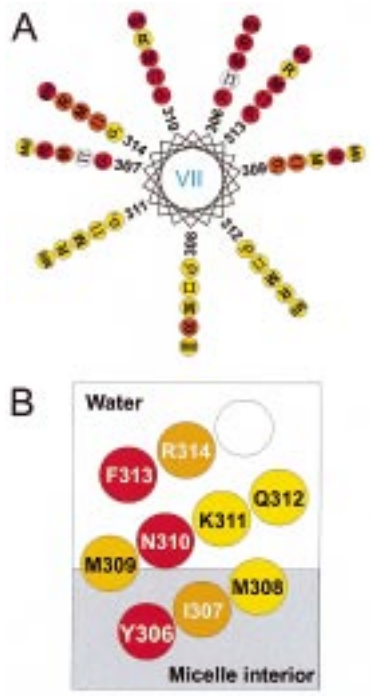

FIGURE 5: (A) A helical wheel representation of the sequence 306−314. For each residue the mobility (M) and accessibilty (Π) are indicated by a graded color scale from red (low values) to yellow (high values). Also shown is the effect of the corresponding cysteine mutation on the activation of G_T (G_T) and on perturbation of the MII lifetime (MII). The magnitude of the effect is also coded on a color scale from red (large effect) to yellow (no effect). Finally, the reactivity of a cysteine at the indicated site (R) is indicated on a color scale from red (low reactivity) to yellow (high reactivity). (B) A helical net representation of the sequence 306−314, showing the location of the micelle−water interface. The color code indicates the mobility and accessibility of the corresponding residue using the code in panel A.

The R1 residues at 306, 310, and 313 are unambiguously located at buried sites in the structure, on the basis of their low mobility (Figure 3, 4) and the low $\Pi(O_2)$ and Π(NiEDDA) of 310R1 and 313R1 (Figure 4). Figure 5A shows that these buried residues with similar EPR spectra are clustered together on a narrow face of the putative helical segment, defining a strongly interacting face of the helix. On approximately the opposite face of the helix, R1 residues at 308, 309, 311, and 312 have a high accessibility and high mobility and define an exposed face of the helix. The EPR spectra of R1 at these sites closely resemble those for this

[2] Φ will be independent of structure only for R1 residues at relatively exposed sites. At buried sites, or sites in strong tertiary interaction, the size difference between O_2 and NiEDDA will result in a steric exclusion of NiEDDA relative to O_2.

side chain at sites on the lipid-exposed surfaces of transmembrane helices in bacteriorhodopsin (*44*) and rhodopsin (*6, 8*).

Residues 307 and 314 are located at the boundary between the strongly interacting and exposed faces of the helix. Accordingly, the spectra of 307R1 and 314R1 are similar, with a complex line shape characteristic of an intermediate mobility (Figure 3). The mobility of 307R1 and 314R1 is lower than generally observed for R1 at either water- or lipid-exposed helix surface sites, and these residues may experience tertiary interactions.

Also mapped onto the helical wheel of Figure 5A are results from a accompanying paper regarding perturbation of G_T activation (G_T), and perturbation of the MII lifetime (MII) produced by cysteine mutations at the same sites investigated here by SDSL (*1*). The magnitude of the perturbation is color coded from red to yellow, with red representing the largest perturbation. Also shown are data on the relative reaction rates for cysteine at the various sites with 4-PDS (*1*), represented by R. Rates are again color coded red through yellow, with red representing the slowest rate.

Figure 5A shows that the sites for which the R1 mobility and accessibility are sharply reduced by interaction with the protein tertiary structure are also sites for which cysteine substitution produces large perturbations in both G_T activation and MII lifetimes. Mutation at sites on the opposite face of the putative helix, the exposed face as defined by SDSL, has essentially no effect on G_T activation or MII. Between these two extremes are intermediate cases as indicated in the figure. Thus, data from four independent measurements display a periodic dependence on sequence position consistent with a α-helical segment in the range from 306 to 314 and, remarkably, with the same relative phase. The fact that the mutation sites that produce maximum perturbation of G_T activation and MII lifetime coincide with tightly packed buried sites as assigned by SDSL is not unexpected. In fact, the correspondence strongly suggests that the effect of the cysteine mutation is due to structural perturbations of the protein, perhaps in the photoactivated state, and not due to simple replacement of a critical functional residue.

Figure 5B shows a helical net representation of the same helix in Figure 5A, identifying the location of the micelle−water interface deduced from the data in Figure 4C. The location of the interface between M308 and M309 is consistent with the amino acid sequence in this region. For example, the preceding sequence from 299 to 308 is largely hydrophobic, while the following sequence contains two charged residues in the next 5 amino acids (Figure 1). Assuming that this assignment for the micelle−water interface holds for the membrane−water interface of the native membrane, helix VII extends approximately 1.5 turns above the membrane surface.

Figure 5A also summarizes some interesting additional data on sulfhydryl reactivity with 4-PDS reported in an accompanying paper (*1*). To a first approximation, the rate of reaction of a sulfhydryl group in a protein should be related to its accessibility to the reagent. However, the accessibility measured in this manner is quite different than that measured by $\Pi(O_2)$ and Π(NiEDDA) for an R1 side chain at the same site. This is seen in Figure 5A at sites 310 and 313. Mutants 310C and 313C have a high reactivity toward 4-PDS, while $\Pi(O_2)$ and Π(NiEDDA) are both very low in 310R1 and 313R1. Thus, SDSL finds these sites to be buried, while 4-PDS reactivity finds them to be relatively exposed. The SDSL assignment appears more attractive in view of the perturbation of the MII lifetime and G_T activation in 310C and 313C, and the extreme immobility of the nitroxides at these sites.

Because these different scales of accessibility must reflect the same equilibrium structure, it seems important to comment on the apparent discrepancy. One explanation can be found in a fundamental difference in the techniques. The EPR measurement is made at equilibrium, and the results reflect the equilibrium structure of the protein molecule. On the other hand, in any sulfhydryl reactivity assay, a successful collision results in the irreversible formation of a covalent bond. The effect is that successive events are "counted", and the method integrates events over time. The above distinction is important for a protein with conformational substates. Consider an example with two conformational substates, only one of which has an exposed sulfhydryl group. If the intrinsic rate constant for reaction with the SH group is high, the product may accumulate at a rapid rate even if the conformation with the exposed group amounts to only a small fraction of the population. The EPR method would not detect the minor population, but would find the SH group to be buried. A combination of SH reactivity and accessibility measured by SDSL provides a more complete picture of the state of the protein than either approach alone. The reactivity provides information of structural fluctuations and local flexibility, while the SDSL measure defines the equilibrium population.

If this explanation is correct, the top portion of helix VII may exist in multiple conformational states, one of which exposes the buried surface occupied by residues 310 and 313. The lack of reaction of 306C with 4-PDS, a residue on the same helix surface as 310C and 313C, may simply be due to limited accessibility of the polar 4-PDS reagent to this site (Figure 5B). The low reactivity at 308C is probably due to the low solubility of 4-PDS in the lipid phase.

Figure 6 suggests a specific mapping of the 306−314 sequence onto the low-resolution electron density maps of frog rhodopsin (*18*), based on the SDSL data presented above. In the figure, the helix model of Figure 5 is superposed on a contoured cross section of the electron density map taken parallel to the membrane plane at distances of 13, 15, and 17 Å from the center of bilayer (data provided by G. F. X. Schertler). This range encompasses the region of the molecule at the membrane−aqueous interface pertinent to the studies presented here (*17*), and the superposition of the layers provides a sense of the helical tilts at this level of the molecule. The circles marking the residues are colored according to mobility/accessibility data using the same code as in Figure 5. The angular position of the helical wheel shown provides a reasonable fit to the salient features of electron density and residue mobility/accessibility data. The strongly immobilized and inaccessible residues 306, 310, and 313 are buried in the core of the molecule. The residues 308R1, 309R1, 311R1, and 312R1 face the outside of the molecule, in contact with either the lipid (308, 309) or the aqueous phase (311, 312), accounting for their high mobility and accessibility. Residues 307R1 and 314R1 are those with intermediate accessibility and mobility (Figures 3 and 4).

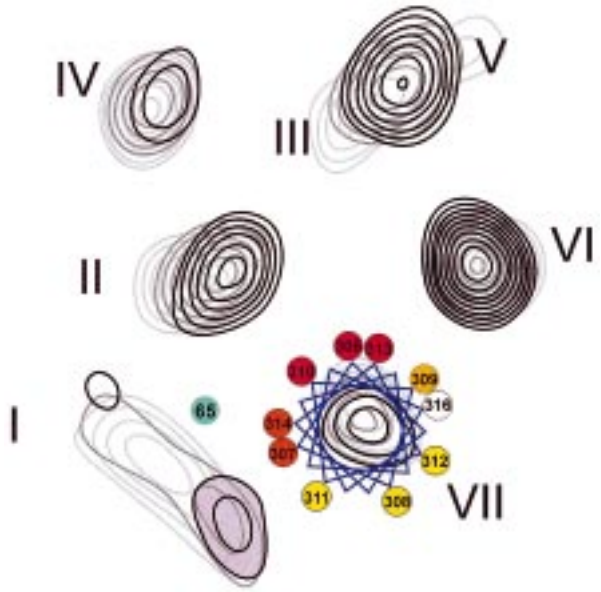

FIGURE 6: Residue positions of the proposed helical segment from 306 to 314 mapped onto electron density contour sections taken at 13, 15, and 17 Å from the center of the membrane. The mobility and accessibility are indicated by the same color code used in Figure 5. The identification of the rhodopsin helices in the electron density map is from refs *17* and *18* and corresponds to the 13 Å section (light contour traces) where the helices are well-resolved. In the 17 Å section (dark contour traces), the densities for helices III and V have merged. The contour sections were from a three-dimensional map at an effective resolution of 7.5 Å in the membrane plane and 16.5 Å normal to the plane and were kindly provided by G. F. X. Schertler (personal communication).

Residue 307R1 is within the bilayer domain and faces an electron density of uncertain origin (violet shading) (*12*). Whatever the origin, the partial immobilization of 307R1 is consistent with the existence of mass in this region. Residue 314R1 is two turns above 307R1 on the same face of the helix but is in the aqueous phase. Although 314R1 directly faces helix I, it has an intermediate mobility rather than the expected strong immobilization. This may be accounted for by the fact that 314 is at the suggested C-terminus of helix VII, and R1 residues at helix C-termini have been found to be unusually mobile (*41*). Overall, the electron density contours and SDSL accessibility/mobility data are compatible for the mapping of the sequences shown in Figure 6.

Baldwin et al. (*17*) proposed a α-carbon structural model for the rhodopsin helices on the basis of a sequence analysis of GPCR's and the electron density map of Unger et al. (*18*). In this model, helix VII crosses the membrane−aqueous interface at residue 307, approximately 17 Å from the center of the membrane, and extends to residue 311. This compares remarkably well with the SDSL data that places the crossing point between 308 and 309 and helix termination near residue 314. Both SDSL and analysis of residue variability among GPCR sequences agree that residues 306, 310, and 313 are buried, while 308, 311, and 312 are located on exposed surfaces of the structure. The α-carbon model, however, places 309 at a buried site, while the EPR spectrum indicates that it is more likely at a surface or contact site.

Recently, the solution structure of a synthetic peptide corresponding to residues 306−348 of native rhodopsin was investigated by 2D NMR (*21*). Remarkably, the peptide had a helical conformation in the region of 306 to approximately 314, in good agreement with the SDSL data.

The structure of the sequence 315−321 cannot yet be determined by SDSL alone. However, the EPR spectra of residues 315R1−317R1 indicate strong tertiary interactions. Moreover, the sulfhydryl groups in 318C, 320C, and 321C are essentially unreactive toward the spin-label reagent (I). Therefore, they are likely to be buried in a rigid part of the molecule, a conclusion already reached from the lack of reactivity of these residues with 4-PDS (*1*). Residue 319 is the only site in the sequence that has a relatively high mobility. Thus, from the point of view of SDSL, the sequence 315−321 is the most sequestered of all the sequences presumed to reside in the aqueous phase at the cytoplasmic surface of rhodopsin (*6*, *8*, *10*, *11*).

Photoactivation of rhodopsin to the MII state produces minor changes in the mobility of R1 throughout the sequence (Figure 3). However, the changes at 306, 313, and 316 are the most notable. The change at 306 is an outward shift of the hyperfine extrema without a significant change in line shape, suggesting that the change may be due to an increase in the polarity of the environment (*42*). The penetration of water, for example, to this site just above the Schiff base in helix VII could produce such a change. The spectral change at 313 is due to a shift in the population of nitroxide to a more mobile state. This is not likely to be due to a movement of helix VII itself, because there is little change at 310R1, one turn below 313 facing helix II instead of VI. However, the outward movement of helix VI previously reported (*8*, *26*) could account for the change, because 313R1 makes tertiary contact with helix VI (Figure 6).

The photoactivated increase in mobility of R1 at 316 has been previously reported (*25*). In addition, residues 316R1 near the end of helix VII and 65R1 in the segment between helices I and II were found to be in close apposition, and photoactivation of rhodopsin results in their separation (*27*). The proximity of 65 and 316 argues against the extension of helix VII to include residue 316. As shown in Figure 6, 316R1 would then be on the opposite side of helix VII, away from residue 65. It seems likely that the part of the sequence 315−321 immediately beyond helix VII is folded over the body of the rhodopsin molecule, where 316R1 can interact with 65R1. This disposition could also account for the lack of reactivity of cysteine residues in this region. The photoactivated motion near 316R1 could result from movement of helix VII, movement of helix I and/or II, or independent movement of the 315−321 segment. The data presented here do not permit a conclusion on this point.

REFERENCES

1. Cai, K., Klein-Seetharaman, J., Farrens, D., Zhang, C., Altenbach, C., Hubbell, W. L., and Khorana, H. G. (1999) *Biochemistry 38*, 7925−7930.
2. Helmreich, E. J. M., and Hofmann, K.-P. (1996) *Biochim. Biophys. Acta 1286*, 285−322.
3. Wess, J. (1997) *FASEB J. 11*, 346−354.
4. Sakmar, T. P. (1998) *Prog. Nucleic Acid Res. Mol. Biol. 59*, 1−34.
5. Ridge, K. D., Zhang, C., and Khorana, H. G. (1995) *Biochemistry 34*, 8804−8811.
6. Farahbakhsh, Z., Ridge, K. D., Khorana, H. G., and Hubbell, W. L. (1995) *Biochemistry 34*, 8812−8819.
7. Yang, K., Farrens, D. L., Hubbell, W. L., and Khorana, H. G. (1996) *Biochemistry 35*, 12464−12469.

8. Altenbach, C., Yang, K., Farrens, D. F., Farahbakhsh, Z., Khorana, H. G., and Hubbell, W. L. (1996) *Biochemistry 35*, 12470−12478.
9. Langen, R., Cai, K., Khorana, H. G., and Hubbell, W. L. (1999) *Biochemistry 38*, 7918−7924.
10. Klein-Seetharaman, J., Hwa, J., Cai, K., Altenbach, C., Khorana, H. G., and Hubbell, W. L. (1999) *Biochemistry 38*, 7938−7944.
11. Altenbach, C., Klein-Seetharaman, J., Khorana, H. G., and Hubbell, W. L. (1999) *Biochemistry 38*, 7945−7949.
12. Kuhn, H., and Hargrave, P. A. (1981) *Biochemistry 20*, 2410−2417.
13. Konig, B., Arendt, A., McDowell, J. H., Kahlert, M., Hargrave, P. A., and Hofmann, K. P. (1989) *Proc. Natl. Acad. Sci. U.S.A. 86*, 6878−6882.
14. Franke, R. R., Konig, B., Sakmar, T. P., Khorana, H. G., and Hofmann, K. P. (1990) *Science 250*, 123−125.
15. Franke, R. R., Sakmar, T. P., Graham, R., and Khorana, H. G. (1992*) J. Biol. Chem. 267*, 14767−14774.
16. Ernst, O. P., Hofmann, K. P., and Sakmar, T. P. (1995) *J. Biol. Chem. 270*, 10580−10586.
17. Baldwin, J., Schertler, G. F. X., and Unger (1997) *J. Mol. Biol. 272*, 144−164.
18. Unger, V. M., Hargrave, P. A., Baldwin, J. M., and Schertler, G. F. X. (1997) *Nature 389*, 203−206.
19. Yeagle, P. L., Alderfer, J. L., and Albert, A. D. (1995) *Biochemistry 34*, 14621−14625.
20. Yeagle, P. L., Alderfer, J. L., and Albert, A. D. (1995) *Nat. Struct. Biol. 2*, 832−834.
21. Yeagle, P. L., Alderfer, J. L., and Albert, A. D. (1996) *Mol. Vis. 2*, 12.
22. Yeagle, P. L., Alderfer, J. L., and Albert, A. D. (1997) *Biochemistry 36*, 3864−3869.
23. Yeagle, P. L., Alderfer, J. L., and Albert, A. D. (1997) *Biochemistry 36*, 9649−9654.
24. Sheikh, S. P., Zvyaga, T. A., Lichtarge, O., Sakmar, T. P., and Bourne, H. R. (1996) *Nature 383*, 347−350.
25. Resek, J. F., Farahbakhsh, Z., Hubbell, W. L., and Khorana, H. G. (1993) *Biochemistry 32*, 12025−12031.
26. Farrens, D. L., Altenbach, C., Yang, K., Hubbell, W. L., and Khorana, H. G. (1996) *Science 274*, 768−770.
27. Yang, K., Farrens, D. L., Altenbach, C., Farahbakhsh, Z., Hubbell, W. L., and Khorana, H. G. (1996) *Biochemistry 35*, 14040−14046.
28. Cai, K., Langen, R., Hubbell, W. L., and Khorana, H. G. (1997) *Proc. Natl. Acad. Sci. U.S.A. 94*, 14267−14272.
29. Kim, J. M, Altenbach, C., Thurmond, R., Khorana, H. G., and Hubbell, W. L. (1997) *Proc. Natl. Acad. Sci. U.S.A. 94*, 14273−14278.
30. Javitch, J. A., Li, Z., Kaback, H. R., and Karlin, A. (1994) *Proc. Natl. Acad. Sci. U.S.A. 91*, 10355−10359.
31. Hubbell, W. L., and Altenbach, C. (1994) *Curr. Opin. Struct. Biol. 4*, 566−573.
32. Hubbell, W. L., Mchaourab, H. S., Altenbach, C., and Lietzow, M. (1996) *Structure 4*, 779−782.
33. Hubbell, W. L., Gross, A., Langen, R., and Lietzow, M. (1998) *Curr. Opin. Struct. Biol. 8*, 649−656.
34. Farahbakhsh, Z., Hideg, K., and Hubbell, W. (1993) *Science 262*, 1416−1420.
35. Sakmar, T. P., Franke, R. R., and Khorana, H. G. (1989) *Proc. Natl. Acad. Sci. U.S.A. 86*, 8309−8313.
36. Zhukovsky, E. A., and Oprian, D. D. (1989) *Science 246*, 928−930.
37. Nathans, J. (1990) *Biochemistry 29*, 4923−4931.
38. Cohen, G. B., Oprian, D. D., and Robinson, P. R. (1992*) Biochemistry 31*, 12592−12601.
39. Robinson, P. R., Cohen, G. B., Zhukovsky, E. A., and Oprian, D. D. (1992) *Neuron 9*, 719−725.
40. Altenbach, C., Flitch, S., Khorana, H. G., and Hubbell, W. L. (1989) *Biochemistry 28*, 7806−7812
41. Mchaourab, H. S., Lietzow, M. A., Hideg, K., and Hubbell, W. L. (1996) *Biochemistry 35*, 7692−7704.
42. Griffith, O. H., Dehlinger, P. J., and Van, S. P. (1974) *J. Membr. Biol. 15*, 159−192.
43. Farahbakhsh, Z., Altenbach, C., and Hubbell, W. L. (1992*) Photochem. Photobiol. 56*, 1019−1033.
44. Altenbach, C., Greenhalgh, D., Khorana, H. G., and Hubbell, W. L. (1994) *Proc. Natl. Acad. Sci. U.S.A. 91*, 1667−1671.

BI9900121